Punctuated actin contractions during convergent extension and their permissive regulation by the non-canonical Wnt-signaling pathway

Hye Young Kim[1] and Lance A. Davidson[1,2,*]

[1]Department of Bioengineering, University of Pittsburgh, Pittsburgh, PA 15260, USA
[2]Department of Developmental Biology, University of Pittsburgh, Pittsburgh, PA 15260, USA
*Author for correspondence (lad43@pitt.edu)

Accepted 20 October 2010
Journal of Cell Science 124, 635-646

doi:10.1242/jcs.067579

Summary

Actomyosin networks linked to the micro-environment through the plasma membrane are thought to be key players in regulating cell behaviors within multicellular tissues, such as converging and extending mesoderm. Here, we observe the dynamics of actin contractions called 'punctuated actin contractions' in the mid-cell body of embryonic mesenchymal cells in the mesoderm. These contraction dynamics are a common feature of *Xenopus* embryonic tissues and are important for cell shape changes during morphogenesis. Quantitative morphological analysis of these F-actin dynamics indicates that frequent and aligned movements of multiple actin contractions accompany mesoderm cells as they intercalate and elongate. Using inhibitors combined with fluorescence recovery after photobleaching (FRAP) analysis, we find that the dynamics of actin contractions are regulated by both myosin contractility and F-actin polymerization. Furthermore, we find that the non-canonical Wnt-signaling pathway permissively regulates levels of punctuated actin contractions. Overexpression of Xfz7 (Fzd7) can induce early maturation of actin contractions in mesoderm and produce mesoderm-like actin contractions in ectoderm cells. By contrast, expression of the dominant-negative *Xenopus* disheveled construct Xdd1 blocks the progression of actin contractions into their late mesoderm dynamics but has no effect in ectoderm. Our study reveals punctuated actin contractions within converging and extending mesoderm and uncovers a permissive role for non-canonical Wnt-signaling, myosin contractility and F-actin polymerization in regulating these dynamics.

Key words: Morphogenesis, Gastrulation, Mediolateral cell intercalation, F-actin, Microfilament, Myosin II, Actomyosin, Contractility

Introduction

The actin cytoskeleton is essential for the mechanical processes driving morphogenesis and tissue remodeling. Dynamic filamentous actin (F-actin) regulates a range of cellular processes, including cell protrusive activity, cell shape change, extracellular matrix (ECM) assembly and tissue stiffness (Lauffenburger and Horwitz, 1996; Wozniak and Chen, 2009; Zhou et al., 2009; Zhou et al., 2010). F-actin polymerization at the leading edge of motile cells serves to extend lamellipodia and filopodia. Rapid F-actin reorganization by polymerization, bundling and branching is controlled by various actin-binding proteins, including myosin II motors, and serves to maintain the mechanical integrity of the cell cortex, to direct cell protrusions and to regulate many events within the cell, such as cytokinesis (Effler et al., 2007; Reichl et al., 2008), apoptosis (Charras, 2008; Rosenblatt et al., 2001; Slattum et al., 2009) and membrane trafficking (Lanzetti, 2007; Liu et al., 2006). Thus, the F-actin cortex within the pericellular regions of the cell might be as important to mechanical processes in cells and tissues as the F-actin involved in cellular protrusions at the leading edge. In epithelial morphogenesis, numerous recent studies have addressed the role of actomyosin dynamics in the apical cortex and adherens junctions; however, the role of actomyosin in shaping mesenchymal tissues, such as mesoderm during convergent extension, remains unclear. Thus, two of the principle functions of actomyosin in cells and multicellular tissues are to physically connect cells with their environment and to drive coordinated cell movements, but how actomyosin accomplishes these functions in vivo during morphogenesis is poorly understood.

Actomyosin is a key target of many gene regulatory networks and signaling cascades that direct morphogenesis. Previous work on *Xenopus* embryonic tissue explants has revealed that F-actin and myosin contractility play crucial roles in cell rearrangement (Skoglund et al., 2008), ECM assembly (Davidson et al., 2008) and tissue stiffness (Zhou et al., 2009; Zhou et al., 2010) during convergent extension. Additionally, dynamic F-actin processes are regulated by polarity factors, such as the non-canonical Wnt or planar cell polarity pathways (Capelluto et al., 2002; Dzamba et al., 2009; Hyodo-Miura et al., 2006; Khadka et al., 2009; Liu et al., 2008; Mlodzik, 2006; Sato et al., 2006; Tanegashima et al., 2008; Tao et al., 1996). Failure or misregulation of the cytoskeleton as cells polarize, assemble matrix, maintain stiffness or generate tractions are likely to underlie the developmental defects responsible for a range of congenital birth defects. Yet, the dynamics of this regulation, where actomyosin contractility occurs and how a 'proper balance' of myosin II contractility and F-actin assembly are established and maintained during morphogenesis are unknown.

To understand the nature of this regulation, we first characterize the dynamics of F-actin networks within the mid-cell cortex in a range of cells in the early *Xenopus* embryo. We then address the questions of what is the 'normal' range of dynamics in cortical F-actin networks and how F-actin polymerization, F-actin bundling and myosin II contractility are responsible for the topological changes seen in the cortical network. We find that dynamic F-actin

Journal of Cell Science

within the cell cortex undergoes stochastic assembly and disassembly over the course of actin contractions. We adopt the term 'punctuated actin contractions' to describe these contractions as they appear analogous to transient actin or myosin assemblies seen during development in invertebrate embryos (Blanchard et al., 2010; Martin et al., 2009; Munro et al., 2004; Velarde et al., 2007). We find that the incidences of contractions are developmentally regulated within the embryo and that the frequency and orientation of punctuated F-actin contractions are modulated by the non-canonical Wnt-signaling pathway during mesoderm cell intercalation.

Results

Transient depolymerization of F-actin in whole embryos results in chronic defects that are similar to defects seen after perturbing the non-canonical Wnt-signaling pathway

Chronic long-term treatment of embryos with F-actin-depolymerizing drugs, such as cytochalasin D or latrunculin B (LatB), is lethal and results in the dissociation of the embryo (Kwan and Kirschner, 2005). Therefore, to begin to understand the role of F-actin in morphogenesis, we investigated the effect of transient inhibition of actin polymerization. We treated batches of embryos with 0.6 μM LatB (Spector et al., 1989), a potent inhibitor of actin polymerization, for a 20-minute period in early gastrulation, rinsed three times in fresh culture medium and then allowed the LatB-pulse-treated embryos to develop. We have previously shown that a brief LatB treatment dramatically diminished the levels of F-actin in whole embryos (Zhou et al., 2009; see figure 6A within). Embryos transiently incubated in LatB developed short axes and sway-back phenotypes (Fig. 1A), similar to those of embryos defective in non-canonical Wnt-signaling. The severity of the convergent extension defects was dependent on the concentration of LatB (Fig. 1B) and the length of treatment (data not shown). Interestingly, we found no indication of a sensitive temporal 'window' for the treatment but, in fact, found similar phenotypes when embryos were pulsed for 20 minutes at any time during early- to mid-gastrulation (from stage 10 to stage 12; data not shown).

The observed developmental defects did not appear to be due to long-term effects on the F-actin cytoskeleton, as F-actin returned to normal levels within 1 to 2 hours (data not shown), but appeared to arise from rearrangements of paraxial mesoderm cells into multi-layered masses, whereas normal paraxial mesoderm formed two distinct sheets (Fig. 1C,D). Such multi-layering of mesodermal tissues is a common defect within embryos defective in the non-canonical Wnt-signaling pathway (supplementary material Fig. S1) (Goto et al., 2005; Wallingford and Harland, 2002; Winklbauer et al., 2001).

The cortical actin cytoskeleton in whole embryos and in explants

In order to understand how the dynamics of F-actin might be responsible for developmental defects in convergent extension we used the actin-binding domain of moesin tagged with GFP (moe–GFP) (Litman et al., 2000) as a reporter for the localization of F-actin in live cells. Using this fluorescent protein reporter we observed remarkable complex F-actin dynamics in a variety of cells within marginal zone explants microsurgically isolated from the embryo and cultured on fibronectin; qualitatively similar dynamics were observed at the basal surface of the animal cap ectoderm, mesoderm and mesendoderm cells (supplementary material Movie 2).

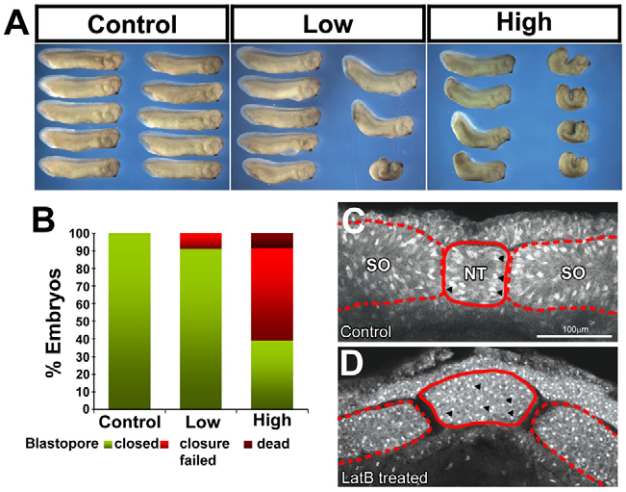

Fig. 1. Transient actin depolymerization results in failure of convergent extension. (**A**) *Xenopus laevis* embryos were transiently treated for 20 minutes during gastrulation with low (0.6 μM) or high (1.2 μM) concentrations of LatB. LatB was washed out and whole embryos were cultured until they reached the tadpole stages. Embryos exposed to a pulse of LatB during mid-gastrulation developed with a short and bent axis in a dose-dependent manner. (**B**) Blastopore closure defects increase with the concentration of LatB. (**C**) Transverse-sectioned dorsal tissue of control embryos show ordered positioning of nuclei within two cell layers in mesoderm (arrowheads). (**D**) Three hours after the LatB pulse and wash, dorsal tissue has randomly positioned rounded cells in multiple layers that thicken both the ectoderm and mesoderm. Cell shapes are visualized by rhodamine–dextran injection at the single-cell stage. SO, somite; NT, notochord.

To verify that moe–GFP reliably reports F-actin within *Xenopus* embryonic cells, we followed two strategies. First, we compared the patterns of F-actin reported by moe–GFP with that reported by phallacidin staining for F-actin in both whole embryos and marginal zone explants (Fig. 2A–B′). Transverse-sectioned whole embryos at mid-gastrulation stage and explants cultured on fibronectin substrate were fixed and stained with BODIPY-FL–phallacidin for static F-actin visualization. Reconstructed *xz* projections from BODIPY-FL–phallacidin-labeled explants showed F-actin-rich protrusions extend over neighboring cells (Fig. 2C) and concentrated F-actin 'spots' on the lateral surface of cells (Fig. 2C″, see arrowheads). F-actin in the cortex underlied the plasma membrane of cells in both developing embryos (Fig. 2A) and isolated tissues. In order to verify that the dynamics of moe–GFP reflected F-actin dynamics, we expressed mRNA encoding a monomeric RFP-tagged version of a different actin-binding domain, isolated from utrophin (Burkel et al., 2007). F-actin dynamics visualized with mRFP–utrophin were similar to those observed with moe–GFP (Fig. 2D) and in mesendoderm fixed and labeled with BODIPY-FL–phallacidin (Fig. 2D′). Thus, with these series of controls, we confirmed that moe–GFP faithfully recapitulates the localization and structure of endogenous F-actin within explants and whole embryos.

Live cortical F-actin undergoes punctuated contractions

Using moe–GFP, we undertook a more rigorous analysis of live-cell F-actin dynamics. Migratory mesendoderm cells typically have a single wide lamellipodium (Davidson et al., 2002; Winklbauer et al., 1996). In our moe–GFP preparations, retrograde flow of F-actin in mesendoderm lamellipodia was clearly visible but so too

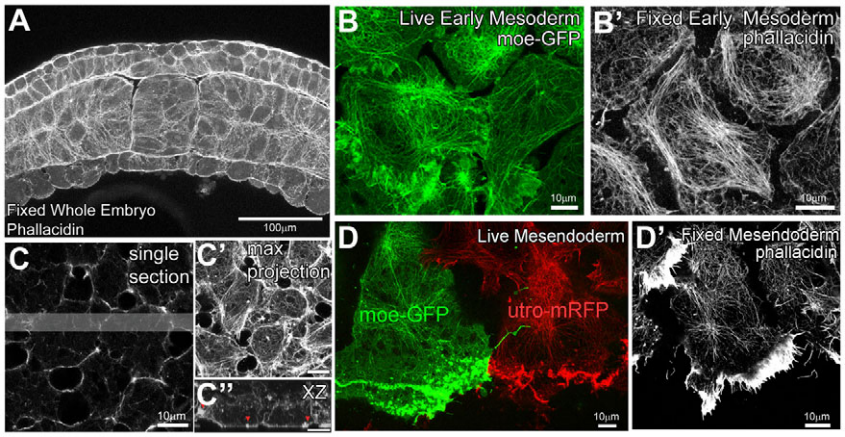

Fig. 2. Cortical actin cytoskeleton. (**A**) Maximum intensity projection of 10-μm thick confocal volumes (20 sections at 0.5 μm intervals) of F-actin stained with phallacidin from a transverse-sectioned whole embryo fixed at stage 12. (**B**) Single confocal image of live early mesoderm cells (at stage 10.5) expressing moe–GFP. (**B′**) A single confocal section of F-actin in fixed early mesoderm cells stained with phallacidin. (**C–C″**) A single confocal section of F-actin within the mid-cell body (C), within fixed animal cap ectoderm stained with phallacidin. (C′) Maximum intensity projection of 3-μm-thick confocal volume collected through the basolateral F-actin cortex. (C″) *xz*-projection showing the lateral F-actin cortex within a 23-μm-thick confocal volume from the shaded region of C. The red arrowheads in C″ indicate dense F-actin networks within the basolateral actin cortex. (**D**) Single confocal image of live mesendoderm cells expressing moe–GFP and utrophin–mRFP. Each cell is the product of a scatter-labeled patch of mRNA-injected cells. The surrounding cells are unlabeled. (**D′**) The F-actin network in fixed mesendoderm cells stained with phallacidin.

were entangled F-actin filaments throughout the cell cortex (Fig. 3H; supplementary material Movie 2). Ectoderm cells also bound fibronectin and sent out protrusions but did not move as rapidly. It is known that mesodermal cells within the embryo, before gastrulation, have few protrusions; at the start of gastrulation they increase their affinity for fibronectin and increase protrusive activity, intercalate between one another and elongate in the mediolateral direction as gastrulation concludes and axis elongation begins (Ramos and DeSimone, 1996; Ramos et al., 1996; Shih and Keller, 1992a; Shih and Keller, 1992b). By the late gastrula stage we observed that the mesodermal cells had elongated along the mediolateral axis [length-to-width ratios (LTW) greater than four were common] and had extended lamellipodia in both medial and lateral directions (data not shown) (Shih and Keller, 1992a). Actin dynamics within *Xenopus* embryonic lamellipodia appeared similar to the actin dynamics in typical motile cells observed in culture (data not shown). In contrast with the stereotypical actin dynamics within lamellipodia, the actin dynamics within the mid-cell cortex were very different and they exhibited unique dynamics within the ectoderm, mesendoderm and mesoderm cell populations (supplementary material Movie 2).

Our observations of complex F-actin dynamics led us to ask a series of questions. First, as the embryonic tissues were cultured on fibronectin substrates, which can limit large-scale cell movements, we wondered whether cortical actin contractions occurred in cells cultured on non-adhesive substrates and whether individual F-actin contractions could alter cell shape. To limit the effect of substrate adhesion on any cortical actin contractions, we used non-adhesive substrates such as agarose- or BSA-coated coverslips (Fig. 3B,C). When cultured on a non-adhesive substrate, cells within a microsurgically isolated tissue (Fig. 3B,B′) and cells within a 'windowed' whole embryo (Fig. 3C,C′) showed similar F-actin dynamics to cells cultured on a fibronectin substrate (Fig. 3G,H). The substrate-free environment enabled cells to deform their neighbors more easily and we found cortical actin contractions correlated with changes of cell shape (Fig. 3D,E; supplementary material Movie 1); as moe–GFP intensity increased, the cell area decreased. The relationship between contraction of the actin cortex and change in cell shape was significantly correlated (the cross-correlation coefficient was –0.89 in the marked cell in Fig. 3C, and the mean value was –0.76 from 12 cells analyzed from three time-lapse movies). Similar observations of actin or myosin regulatory light chain dynamics and their effect on cell shape have been reported during epithelial morphogenetic movements in *Drosophila* (Blanchard et al., 2010; Martin et al., 2009) but have not been observed previously during vertebrate morphogenetic movements. We conclude that punctuated actin contractions generate sufficient force to deform cells in the embryo, but have a more limited effect when cells are more firmly bound to fibronectin-coated substrates.

We next wondered whether cell–cell contact in embryonic tissues induced actin contractions. To investigate this question, we dissociated mesoderm cells from marginal zone explants (Fig. 3F) in Ca^{2+}- and Mg^{2+}-free Danilchik's For Amy (DFA) medium, moved the cells back into DFA and cultured them on a fibronectin substrate. In this way we obtained two- and three-cell clusters, as well as single cells, on fibronectin (Fig. 3G). Although the cell clusters had F-actin arrays denser than those in single cells, we could easily observe F-actin contractions within both populations. Use of substrate-free culture and observation of F-actin contractions within dissociated cells confirmed the importance of punctuated F-actin contractions in guiding cell shape change. For the remainder of the study, we used explants cultured on fibronectin as cell behaviors are well-characterized in these explants and the actin cortex is optimally positioned for confocal imaging.

We then returned to our examination of actin contractions within ectoderm, early mesoderm and late gastrula stage mesoderm found in marginal zone explants. Early gastrula stage mesoderm cells showed complex assemblies of entangled F-actin within mid-cell regions, as well as in lamellipodia, as cells began to intercalate between each other (Fig. 3H; supplementary material Movie 2). At later gastrula stages, we observed alignment of cortical F-actin to the mediolateral axis (Fig. 3H; supplementary material Movie 2),

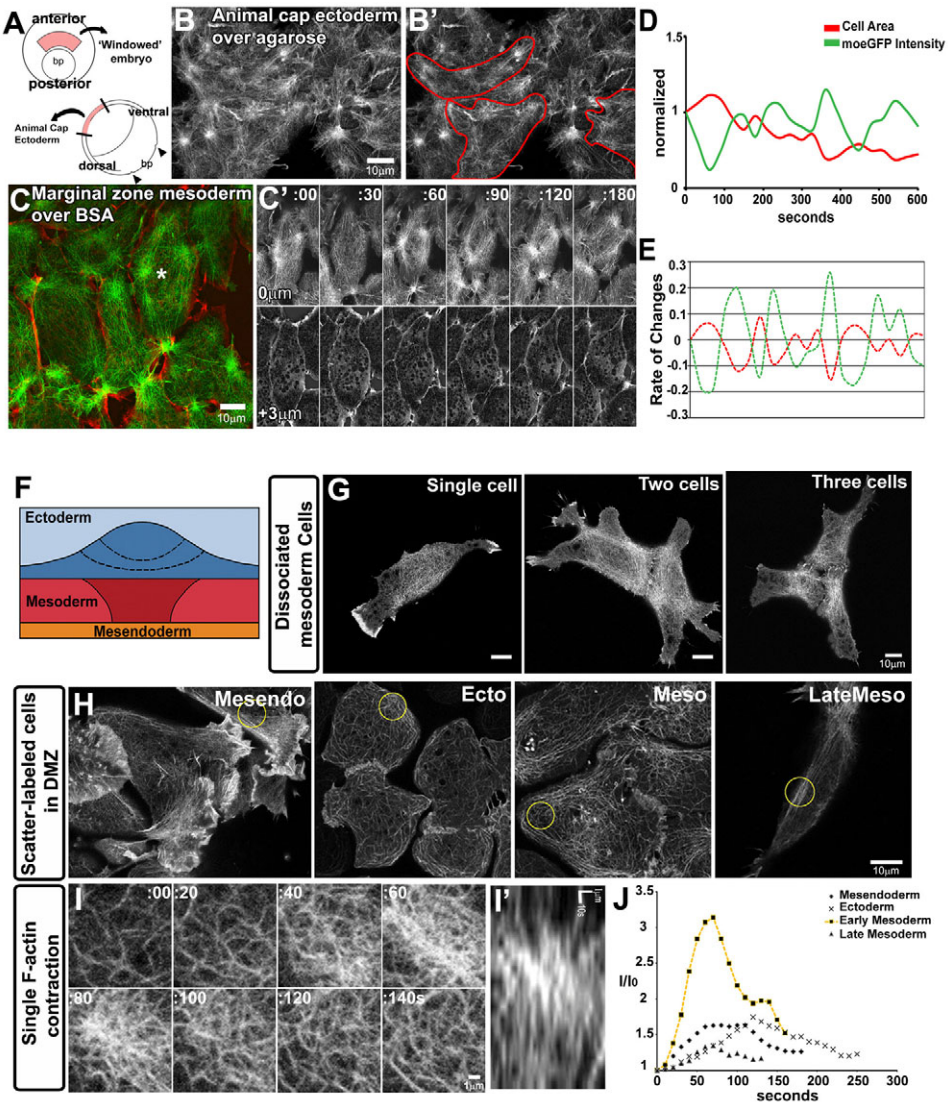

Fig. 3. Punctuated F-actin contractions regulate cell shape. (**A**) A schematic of the gastrula from the vegetal view (left) and sagittal view (right). bp, blastopore. Mesoderm cells (pink) are exposed by removing the epithelial sheet from the embryo, to give the 'windowed embryo', in order to observe the dynamics of cells and F-actin (as shown in C). Confocal images from a time-lapse movie of moe–GFP-expressing animal cap ectoderm on agarose (**B**,**B′**) and marginal zone mesoderm from the windowed embryo (**C**,**C′**). Confocal sections were taken at two depths, either for the F-actin cortex (green) or for the cell outline (red), in order to capture the dynamics of both cell behaviors and F-actin. C′ shows images from the time-lapse movie of the marked cell in C. (**D**) The cell area is inversely correlated with the moe–GFP intensity from the cell (results are from the marked cell in C). As the area of the cell decreases (or cells contract their body), the moe–GFP intensity increases (the F-actin network gets tensed). (**E**) The mean cross-correlation coefficient for the rate of changes between the cell area and the moe–GFP intensity is –0.76 (12 cells from three time-lapse movies). (**F**) A fate map of the marginal zone explant. (**G**,**H**) Confocal images of moe–GFP from dissociated mesoderm cells and cells in the dorsal marginal zone (DMZ) tissue, including mesendoderm, ectoderm, early mesoderm and late mesoderm cells. (**I**) A time series of confocal images of a single cortical F-actin contraction within an early mesoderm cell. (**I′**) Kymograph of intensities through the mid-line of the same contraction as in (I). (**J**) Moe–GFP intensity profiles in the circular region of (B–D) for one episode of F-actin contraction shown as the normalized intensity (I/I_0; I_0 is initial intensity) within a circular region of each cell type (yellow circles in the scatter-labeled cells in H) over a single contraction.

as has been previously reported (Skoglund et al., 2008). For comparison, we also observed actin dynamics within the mid-body cortex of ectoderm cells; these cells had a relatively sparse F-actin network and showed few F-actin contractions (Fig. 3H; supplementary material Movie 2). In fact, cortical actin contractions could be found throughout the embryo, for example in ventral mesoderm cells from isolated explants and animal cap cells, as early as the mid-blastula transition (stage 8; supplementary material Fig. S2). However, distinct changes in F-actin dynamics paralleled changes in cell behaviors from cell-type to cell-type and from stage to stage.

In contrast with the changing cell-scale pattern of contractions, the kinetics of single F-actin contractions appeared similar in a variety of cells and stages. We refer to this single cycle as a 'punctuated F-actin contraction' (see a representative punctuated F-actin contraction in Fig. 3I; supplementary material Movie 3). During a punctuated F-actin contraction, the sparse background of F-actin increased in density as F-actin gathered towards a focal point then dispersed over several minutes (Fig. 3I′). Close inspection of other time-lapse sequences using selected regions of cortical F-actin [circular regions of interest (ROIs) in Fig. 3H] revealed similar patterns of F-actin dynamics in mesendoderm, ectoderm and mesoderm (Fig. 3J). The intensity of F-actin over a single episode of contraction in different cells exhibited similar patterns of accumulation and dissipation, lasting from 60 to 120 seconds. Thus, using validated live reporters of F-actin dynamics we showed punctuated F-actin contractions within the cell cortex and that contractions are a common feature shared by a variety of different cell types in *Xenopus laevis* embryos.

Punctuated F-actin contractions increase in frequency and align within elongated cells

Although the observed single punctuated F-actin contraction was similar among cell types within the marginal zone, we suspected that mesoderm cell elongation was driven by accumulated patterns of multiple contractions that together push or pull the cell body, as well as neighboring cells. Our initial attempts to analyze the punctuated F-actin contractions with intensity profiles or kymographs of cortical F-actin contractions at fixed positions allowed us to characterize the formation of F-actin contractions (Fig. 3I–J); however, these qualitative methods could not adequately describe the physical dynamics of the punctuated F-actin

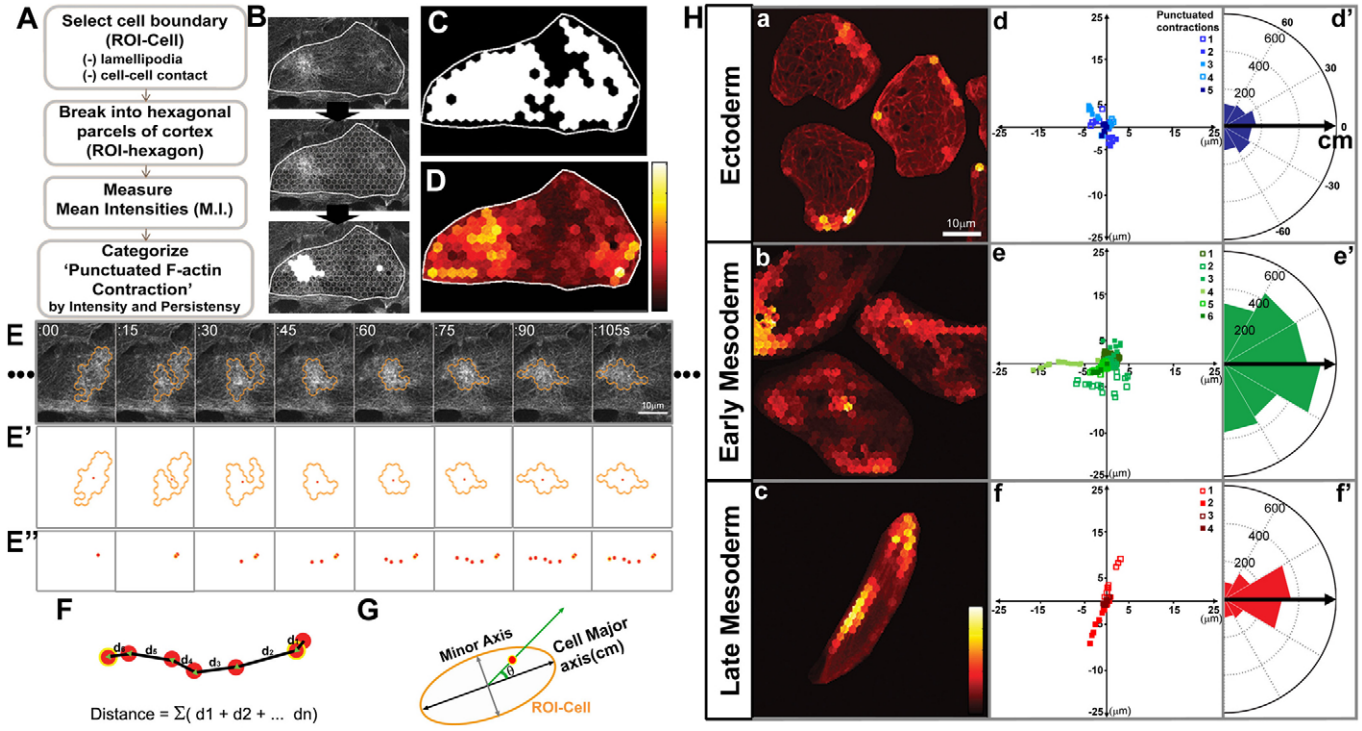

Fig. 4. Quantitative analysis of contraction morphology. (**A**) Flow-chart for the image-processing steps used to identify the contractile actin cortex and categorize the individual punctuated F-actin contraction. (**B**) The identifying steps applied on a live-cell moe–GFP confocal image of an anterior mesoderm cell. The cell boundary of the selected cell (ROI-Cell) is shown with a white line, which is divided into hexagonal parcels (ROI-hexagon). White-filled ROI-hexagons are the identified ROI-hexagons containing 'active' actin cortex. (**C**) The contractile area displays the region where a contractile F-actin cortex was present in at least a single frame during the 30 minutes. (**D**) The incident frequency of F-actin contractions in each ROI-hexagon is shown by the F-actin frequency map. A 30-minute time-lapse was used for C and D. (**E**) A time-lapse movie following moe–GFP identifing punctuate F-actin contractions. (E′–E″) The identified positions (red dots) of the center of intensity of a categorized actin contraction enclosed by the hexagonal area. (**F**) The distance of movements is the sum of segmented distances for one episode of an F-actin contraction. (**G**) Anglular distributions of the positions of F-actin contractions with respect to the major cell (cm) axis represented by angle θ. (**H**) (a–c) F-actin frequency maps from a confocal time-lapse movie of moe–GFP-expressing ectoderm (a), early mesoderm (b), and late mesoderm (c) cells. (d–f) Scatter plots display relative movement vectors of F-actin contractions from one representative cell starting from its origin (0,0). (d′–f′) Circular histograms represent the angular distribution of the punctuate F-actin contractions with respect to the cell major axis. (see G for the method: the major cell axis is set to 0, the angle between the F-actin contraction and the major cell axis is θ). The heat-map colors in (D) and (H) indicate an arbitrary frequency scale from high frequency or high persistence 'light' to low frequency or low persistence 'dark' (see supplementary material Tables S1 and S2 for a summary of the quantified punctuated F-actin contractions).

contractions or suggest how these structures might be controlled or localized. To get a better understanding of the complex dynamics of the F-actin contractions, we assessed contraction movements, and their frequency and localization, by quantitative image analysis.

To investigate the temporal and spatial dynamics of punctuated F-actin contractions that form moving structures akin to unitary sites of focal adhesions, we adapted image-processing tools appropriate to tracking discrete objects in cells (Fig. 4A). In order to detect fluctuations of F-actin intensity over time within the mid-cell cortex and to track dynamics of individual punctuated F-actin contraction events, we first manually selected a large region within each cell from a single frame in a 10-minute confocal time-lapse sequence. The selected ROI contained the cell mid-body and excluded lamellipodia and cell–cell contacts (ROI-Cell). The ROI-Cell was then subdivided into small hexagonal units; each ROI-hexagon was 2.4 μm in diameter and contained ~270 pixels. The hexagonal shape was chosen to register the presence of multiple actin filaments or bundles and track these cytoskeletal elements as a contiguous structure once an F-actin network contracts. To classify the status of F-actin within the hexagon, we compared the F-actin intensity within the hexagon with the mean intensity within the ROI-Cell. In the first round of analysis, hexagons were classified as 'contraction-active' if the F-actin signal intensity within the ROI-hexagon was greater than 150% that of the mean intensity of the ROI-Cell (Fig. 4B). At this stage in the analysis, each contraction-active hexagon represented a small patch of contracted F-actin cortex within a single image.

Given that F-actin contractions could extend over large areas of the cell, persist for several minutes and change shape, we extended the classification scheme to connect multiple contraction-active hexagons within a time-lapse sequence. First, we developed a decision flow-chart to assign ROI-hexagons into multi-hexagon patches within the same frame. Next, we extended the flow-chart logic to bridge small temporal gaps in the history of a single hexagon over the course of a single punctuated F-actin contraction. In brief, in order for an ROI-hexagon to be included in a punctuated F-actin contraction, a contraction must be: (1) seen in three contiguous hexagons; (2) persist for at least 30 seconds; and (3), to be counted as the same event, multi-hexagon contractions must overlap from frame to frame. Given the stringent contraction threshold of 150%, we merged single transiently non-contractile hexagons into punctuated contractions if they were completely

bounded by contractile hexagons. This segmentation process allowed us to identify and track high-density regions of F-actin cortex (Fig. 4E–E″) from the formation of a contraction to its disappearance, providing information on how punctuated F-actin contractions moved as they formed, spread and contracted.

In addition to tracking formation and movements of single contractions, our analysis measured the frequency of punctuated contractions within the mid-cell cortex and identified subcellular domains where multiple contractions occurred. Contractility within a cell was reported as a contractile area (Fig. 4C) or was displayed in an F-actin contraction frequency map (Fig. 4D). Contractile area was defined as the total area covered by punctuated contractions over the course of the time-lapse. In contrast with the morphological identification of multi-hexagon contraction events, the frequency map reported the chances of finding contractile F-actin within each hexagon. To highlight the relative levels of F-actin contractions within a cell cortex, the F-actin frequency map calculated the average 'contractility' for each ROI-hexagon in the ROI-Cell and tracked the chance of contraction within any particular hexagon. The orientations of punctuated F-actin contraction movements were measured with respect to the major cell axis (Fig. 4G) and were plotted in a circular histogram (see Fig. 4Hd′, e′ and f′; see also supplementary material Fig. S3). This image analysis procedure allowed us to quantify the lifetimes, frequencies and movements of punctuated F-actin contraction and to compare and contrast these features of F-actin dynamics across a variety of cell types, developmental stages and treatments.

As mesoderm cell shapes progress from isodiametric to mediolaterally elongate over the course of convergent extension, we wondered whether cortical F-actin dynamics are also varying in different cell types and developmental stages. To examine correlations between punctuated F-actin contractions and distinct cell behaviors, we first compared the pattern of punctuated F-actin contractions using frequency maps constructed from 10-minute confocal time-lapse sequences of moe–GFP collected from different regions within marginal zone explants (Fig. 4Ha–c, from ectoderm, early mesoderm, and late mesoderm cells, respectively; supplementary material Table S1).

We found very different frequency maps among the cell populations. Small patches of intermediate-intensity hexagons along the edge of ectoderm cells showed that these regions contained fewer F-actin contractions (Fig. 4Ha) in contrast with those found in early mesoderm cells, which included a large number of F-actin contractions (Fig. 4Hb). The frequency of contractions in late mesoderm cells displayed an equally distinctive pattern; highly persistent F-actin contractions formed running parallel to the major cell axis (Fig. 4Hc). Given that both punctuated contractions and lamellipodial protrusions aligned to the cell, we hypothesized that punctuated F-actin contractions might play a role in elongating mesoderm cells.

To investigate the role of punctuated contractions in shaping cells, and whether the movements of individual F-actin contractions could account for patterns in the frequency map, we tracked contraction positions as they formed, moved and disappeared. Trajectories of the movement of the centers of punctuated contractions from one representative cell in each population showed that contractions could move either randomly or in distinct patterns (Fig. 4Hd, e and f). The infrequent contractions within ectoderm cells moved in random directions and did not move far from their initial site of formation (11.42±7.38 μm per contraction; 17 cells). By contrast, the punctuated F-actin contractions moved larger distances in both early (18.50±21.03 μm per contraction; 17 cells) and late mesoderm (18.49±25.62 μm per contraction; 14 cells).

The movements of punctuated F-actin contractions in mesoderm cells changed during gastrulation. In late gastrula mesoderm cells, individual punctuated F-actin contractions appeared to move back and forth, oscillating along the same path, whereas in early mesoderm and ectoderm cells they moved randomly (Fig. 4Hd,e and f). Given that mesoderm cells elongate from early- to late-gastrula stages, we suspected that the orientation of punctuated F-actin contraction movements was related to the elongation of the cell. To test our hypothesis, we measured the LTW ratio and the angle (θ) of F-actin contraction movements with respect to the major axis of the cell. Even though some early mesoderm cells elongate to a LTW greater than 2, we found movements of punctuated F-actin contractions aligned with the major cell axis only in late mesoderm cells (Fig. 4Hd′,e′ and f′; supplementary material Fig. S3). By contrast, punctuated F-actin contractions did not move parallel to the major cell axis in either ectoderm or early mesoderm cells. These results indicate that individual punctuated F-actin contractions move along the major cell axis only within late gastrula mesoderm cells; furthermore, contraction movements need not be aligned with the major axis of the cell.

Regulation of cortical F-actin contractions

To test the separate roles of actin polymerization and myosin contractility in the formation of punctuated F-actin contractions, we used small-molecule inhibitors and protein overexpression to alter F-actin dynamics in early mesoderm cells, before the cells had adopted a strong mediolateral bias to their shape and behavior.

To depolymerize or stabilize F-actin, we treated marginal zone explants with 0.6 μM LatB or 5 μM jasplakinolide (Jas), respectively, or we overexpressed the Lim kinase mutant LimK T508EE ($LimK^{CA}$), which has been reported previously to phosphorylate cofilin and increase the assembly of F-actin (Edwards and Gill, 1999; Mseka et al., 2007). To increase or inhibit myosin-II-induced F-actin contractions, 50 nM calyculin A (CalA), a myosin light chain phosphatase inhibitor, or 50 μM Y27632 (a Rho-kinase inhibitor), respectively, were used. Each inhibitor treatment dramatically changed the F-actin network within 60 to 90 minutes. Mesoderm cells treated with CalA exhibited dense F-actin arrays that moved back-and-forth around the cell periphery, as well as across the cell cortex. These rapid movements occured in the absence of normal sheet-like lamellipodial protrusions (Fig. 5A; supplementary material Movie 4). By contrast, treatment with Y27632 did not affect lamellipodial protrusions but resulted in fewer punctuated F-actin contractions (Fig. 5A; supplementary material Movie 4). Incubation with Jas caused rapid aggregation of F-actin into a few large focal points within cells. Surprisingly, treatment with Jas and LatB both result in the formation of F-actin aggregates that appeared stabilized at specific sites within the cell. The constitutively active LimK induced large star-like F-actin structures within dense F-actin networks. Given that single images of F-actin distribution reveal only gross morphology, we processed short-duration time-lapse sequences into maximum-intensity projections to highlight regions where repeated F-actin contractions appeared as dense persistent networks (see T-projections in Fig. 5A); regions of high intensities in projected time-lapse sequences could indicate regions with either more frequent contractions or where contractions were more persistent after cells were incubated in either CalA or Jas, as well as increased numbers of contractions within $LimK^{CA}$-expressing cells. Low-intensity regions in time-

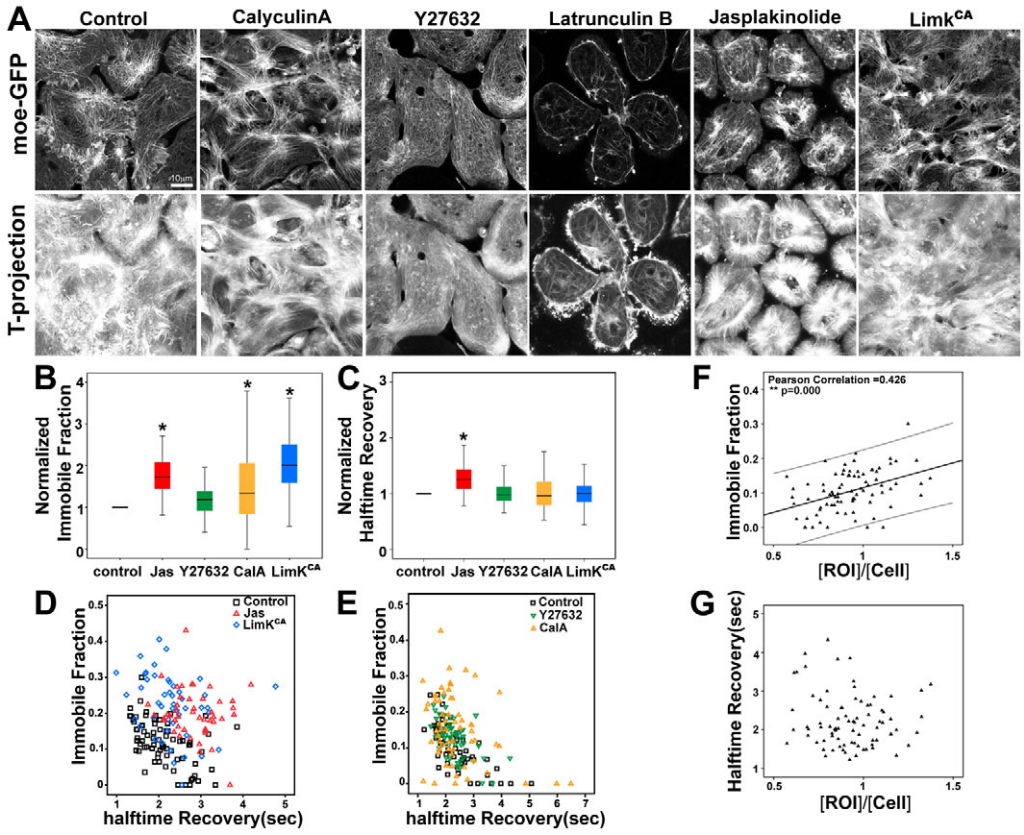

Fig. 5. Formation of punctuated F-actin contractions on perturbation of myosin contractility and filamentous actin kinetics. (**A**) Confocal images from a representative time-lapse sequence of moe–GFP-expressing early mesoderm cells treated with 50 nM CalA, 50 µM Y27632, 0.6 µM LatB, 5 µM Jas or expressing LimK^{CA}. The maximum projection of the time-series of moe–GFP shows the overall levels of F-actin dynamics for 10 minutes during early gastrulation. (**B**) The immobile fraction (*P<0.001, 56 control and 46 Jas-treated cells) and (**C**) halftime recovery (*P<0.001, 56 control and 46 Jas-treated cells) are significantly higher in Jas-treated cells than in control cells. (**D**) Jas-treated cells have significantly higher values for the halftime recovery and immobile fraction compared with control cells. (**E**) Both Y27632- or CalA-treated cells have similar ranges for both immobile fraction and halftime recovery compared with control cells. (**F**) The F-actin-rich cortex has a higher immobile fraction after photobleaching within control cells. The *x*-axis represents the ratio of moe–GFP intensity in the bleached region to the intensity over the entire cell before photobleaching. For control cells, the pre-bleach intensity levels of the bleach area are positively correlated with the immobile fraction [Pearson correlation=0.426 (a slope with 95% confidence interval); **P<0.001, 82 control cells], but shows no correlation with the halftime recovery (**G**). Note that the immobile fractions (B) and time recovery (C) were normalized to controls in order to compare the different treatments. Raw values for are shown in (D) and (E).

lapse projections indicated where contractions are less frequent or less persistent following Y27632 or LatB treatment.

In addition to assessing the morphological changes of actin filaments induced by inhibitors, we monitored the biochemical consequences of these treatments on actin filaments using fluorescence recovery after photobleaching (FRAP) (Amato and Taylor, 1986; Axelrod et al., 1976). Fluorescence recovery of moe–GFP was monitored after photobleaching a 7-µm-by-7-µm region of F-actin cortex within mesoderm cells treated with Jas, Y27632 or CalA, as well as in cells expressing LimK^{CA} (see the Materials and Methods section). FRAP analysis reports the amount of fluorescence that does not recover after bleaching as the ‘immobile fraction’ and the time-scale needed to re-establish the labile fluorescence fraction as the ‘recovery time’. Cells incubated with Jas showed a substantially increased immobile fraction, as well as increased recovery times (Fig. 5B,C), indicating that Jas stabilized F-actin (Fig. 5D). Similarly, cells expressing LimK^{CA} had stabilized F-actin, with a substantially increased immobile fraction (Fig. 5B). Our FRAP data suggest that F-actin aggregates in Jas-treated and LimK^{CA}-expressing cells are the result of either enhanced actin polymerization or suppressed actin depolymerization. LimK^{CA} did not disrupt the F-actin morphology as severely as Jas, but our FRAP analysis indicates that it has similar effects to Jas on the stability of F-actin. This difference might be in part due to the unique targeting of LimK and cofilin in embryonic cells, whereas Jas might exert global effects on all manner of actin-dependent processes within cells. By contrast, the stability of F-actin in cells treated with inhibitors that modulate myosin activity (Y27632 or CalA) was not altered from that in controls (Fig. 5B,C and E), even though these inhibitors produced noticeable changes in the morphology of F-actin (Fig. 5A).

It is worth noting that there was considerable variation in the FRAP results within control cells. We wondered whether this variation could be due to heterogeneities in the network morphology, for instance owing to differences between contractile and non-contractile regions. To test this, we compared FRAP results between these regions and found that increases in the immobile fraction within control samples were significantly correlated with the relative initial intensity of the moe–GFP of the photobleached region (Fig.

5F; Pearson correlation=0.426; $P<0.000$). This suggests that the punctuated contractions contained a more stable cortex than non-contracting regions. Alternatively, a contractile cortex could be affecting the calculation of recovery dynamics through movement of unbleached F-actin into, or polymerizing more F-actin within, a forming contraction. We also found that F-actin contractions induced by CalA (Fig. 5B) exhibited a large variance in the immobile fraction. However, regions undergoing punctuated actin contractions did not show altered recovery times (Fig. 5G). Owing to the technical limits of confocal scanning and the short lifetime of F-actin contractions, we were not able to resolve differences between the assembly and disassembly phases of punctuated contractions. Thus, evidence from the inhibitor and FRAP studies revealed that punctuated F-actin contractions are the product of coordinated actin polymerization and myosin II activity and that these processes underlie the developmental regulation of the frequency, duration and movement of contractions within cells.

Non-canonical Wnt-signaling regulates punctuated F-actin contractions

Given that punctuated F-actin contractions regulate cell shape change, and that actomyosin regulation is a direct target of the non-canonical Wnt-signaling during convergent extension in the frog, we were interested in the role of Wnt signaling in modulating these contractions. To investigate the role of non-canonical Wnt-signaling on actin contractions we chose to alter signals from either the frizzled (Fzd) receptor or the disheveled (Dsh) cytoplasmic protein. Given that Xfz7 (Fzd7) is only expressed within involuting mesoderm cells during gastrulation and that it is thought to mediate mediolateral cell intercalation behaviors (Djiane et al., 2000), we hypothesized that we could activate punctuated actin contractions by expressing Xfz7 in animal cap ectoderm cells. By the same logic, expression of Xdd1, a mutant form of *Xenopus* Dsh that inhibits convergent extension, would reduce the number of contractions within mesoderm cells.

To track F-actin dynamics in live cells, we coinjected mRNA encoding moe–GFP and either Xdd1 or Xfz7 and collected confocal time-lapse images from moe–GFP-expressing cells within marginal zone explants during gastrulation. We expressed these mRNAs at levels that consistently produced moderate whole-embryo phenotypes comprising the shortened anterior–posterior axes and defects in neural tube closure shown in previous studies (Djiane et al., 2000; Wallingford et al., 2000). Overexpression of Xfz7 increased the frequency of punctuated F-actin contractions by increasing the stability of the F-actin network. Animal cap ectoderm cells expressing Xfz7 developed dense arrays of contracting actin networks in the mid-cell cortex compared with those in control cells (Fig. 6B; supplementary material Movie 6). In fact, the rate of punctuated F-actin contractions was increased 4.6-fold in Xfz7-expressing ectoderm cells, which also had similar rates of contractions to those in control mesoderm cells (Fig. 6G). Overexpression of Xfz7 in mesoderm cells induced persistent contractions with a longer lifetime than those in control cells (Fig. 6H; supplementary material Table S2), and the cells that were less elongated (LTW 1.51±0.22; 12 cells from four explants) than control cells (LTW 2.11±0.84; 12 cells from four explants) (Fig. 6A; supplementary material Movie 5). FRAP analysis of F-actin within Xfz7-expressing mesoderm cells indicated that Xfz7-induced actin networks comprised arrays of F-actin that were more persistent (Fig. 6D,E) and similar to those observed after CalA treatment (Fig. 5B,C). Thus, expressing exogenous Xfz7 receptors in animal cap ectoderm increases the frequency of actin contractions to the levels seen in mesoderm, whereas increasing expression of Xfz7 receptors in mesoderm cells that already express Xfz7 induces more persistent contractions that comprise more stable F-actin.

To test whether downregulation of the non-canonical Wnt-signaling pathway could reduce punctuated contractions, we expressed Xdd1 in mesoderm cells. Overexpression of Xdd1 in mesoderm cells can inhibit cell elongation, so that, by late gastrulation, Xdd1-expressing mesoderm cells retained a rounded shape (LTW 1.44±0.24; 15 cells from five explants) compared with the shape of control mesoderm cells (LTW 4.13±1.72; 12 cells from seven explants) (Fig. 6G). Overexpression of Xdd1 blocked the changes in the frequency and oriented movement of the punctuated F-actin contractions typically seen in the dorsal mesoderm. Mesoderm cells expressing Xdd1 retained similar levels of F-actin to control cells, both in mid-cell cortex and lamellipodia, but the frequency of punctuated F-actin contractions was reduced to less than half the frequency of the punctuated F-actin contractions found in control cells (Fig. 6C,G; supplementary material Movie 5). Furthermore, F-actin contractions in Xdd1-expressing cells moved in random directions, whereas the more frequent punctuated F-actin contractions in control cells moved parallel to the cell axis of elongated mesoderm cells (Fig. 6C). To rule out the possibility that overexpression of Xdd1 globally alters actin dynamics, we expressed moe–GFP and Xdd1 in animal cap ectoderm. Xdd1 had no effect on ectoderm cell shape (Fig. 6F). Punctuated F-actin contractions normally found in animal cap ectoderm cells showed no distinct patterns in movement. When applying the same image-analysis tools that we used for the mesoderm, we found no differences between either contractile area, rate of contraction or direction of movement when we compared F-actin dynamics within control ectoderm cells with Xdd1-expressing ectoderm cells (Fig. 6B and F–H; supplementary material Table S2).

Discussion

Cells in developing *Xenopus* embryos contain a complex and dynamic F-actin-rich cortex. To describe this network during morphogenesis, we used moe–GFP to label tissues for live-cell confocal imaging. We found rapidly moving F-actin features, referred to here as punctuated F-actin contractions, within the cell cortex, and then compared contraction dynamics in different cell types. Static and less-frequent punctuated F-actin contractions were present in ectoderm cells, whereas contractions were more frequent in mesoderm cells and moved over larger distances than contractions in ectoderm. Furthermore, contractions in early mesoderm and ectoderm were randomly oriented but switched to move parallel to the longest axis of the cell at later gastrula stages.

We also investigated how the dynamics of punctuated F-actin contractions were regulated by the non-canonical Wnt-signaling pathway. Expressing Xfz7 receptors alone in animal cap ectoderm increased the frequency of punctuated contractions and the stability of the resulting F-actin network to the levels seen in the early mesoderm. Overexpression of Xfz7 in mesoderm also enhanced the rate of contractions and their lifetime. In effect, Xfz7 overexpression made the F-actin network mesoderm-like in ectoderm cells and matured the nascent F-actin in early mesoderm into the dense networks of late mesoderm. By contrast, expressing the dominant-negative disheveled protein Xdd1 in mesoderm

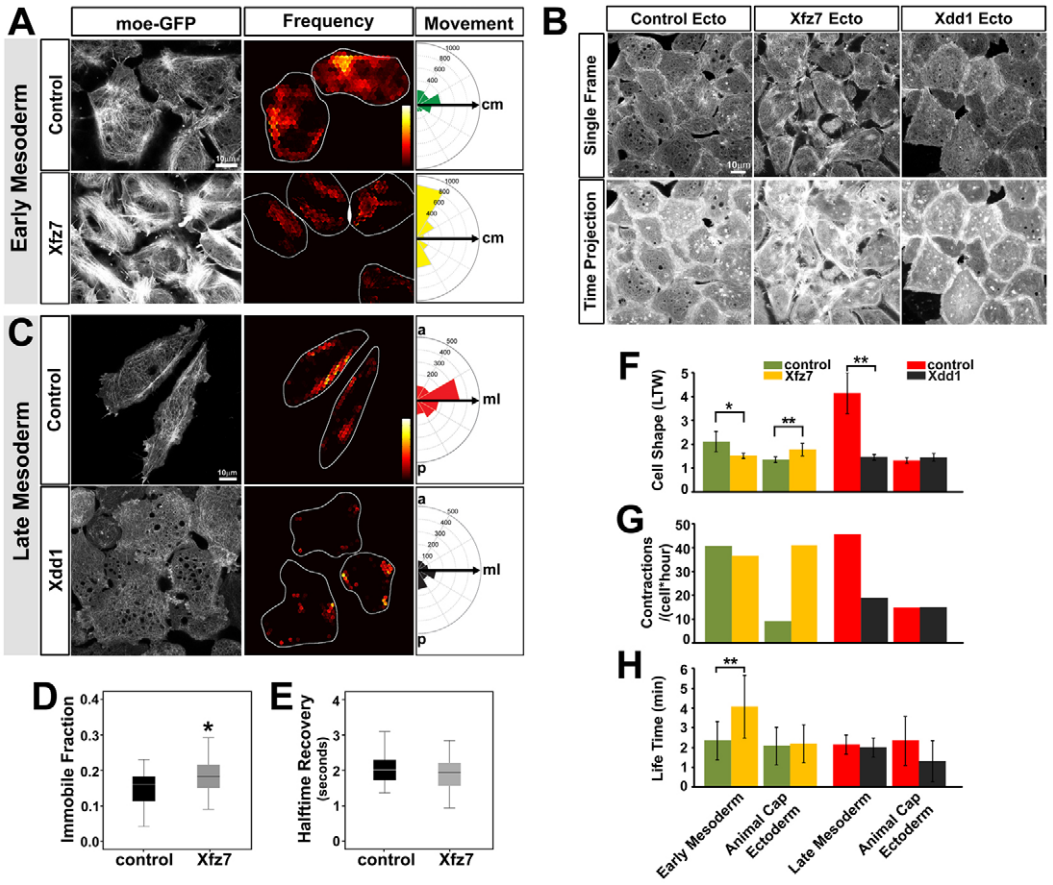

Fig. 6. Punctuated F-actin contractions are modulated by non-canonical Wnt-signaling. The dynamics of punctuated F-actin contractions are compared in cells where non-canonical signaling is reduced by Xdd1 or where signaling is stimulated by Xfz7. (**A**) Punctuated F-actin contractions in moe–GFP-expressing early mesoderm cells (control and Xfz7-expressing cells) exhibit different patterns of frequency and direction of the movements (cm, cell major axis). Note that the calculated orientation of punctuated F-actin contractions from round cells, such as Xfz7-expressing cells (LTW 1.51±0.22) (see supplementary material Tables S1 and S2) are not meaningful when compared with the contraction orientations in elongated cells, such as the late mesoderm cells in (C) (LTW 4.13±1.72). (**B**) Animal cap ectoderm cells expressing moe–GFP (control, and Xfz7- or Xdd1-expressing cells) and maximum projection of 10-minute time-lapse sequences. (**C**) Punctuated F-actin contractions in moe–GFP-expressing late mesoderm cells (control and Xdd1-expressing cells) exhibit different patterns of frequency and direction of the movements. ml, mediolateral axis. (**D**,**E**) Xfz7-expressing early mesoderm cells have a significantly high immobile fraction than in control cells. (**F**–**H**) Quantified results of cell shape, rate and the lifetime of punctuated F-actin contractions from Xfz7- or Xdd1-expressing cells. *P<0.05; ** P<0.01 (see supplementary material Tables S2 and S3). The heat-map colors in (A) and (C) indicate an arbitrary frequency scale from high frequency or high persistence ‘light’ to low frequency or low persistence ‘dark’.

cells reduced the numbers of punctuated actin contractions and blocked their alignment. This latter effect could be due to the abrogation of planar cell polarity cues or alternatively could have abrogated reception of other planar cues that have not yet been identified. Several other sources of planar cues, independent of non-canonical Wnt-signaling pathways, have been implicated in germband elongation (Zallen and Wieschaus, 2004) and elongation of the forming oocyte in *Drosophila* (Frydman and Spradling, 2001; Viktorinova et al., 2009) and might underlie elongation of *Xenopus* multicellular aggregates (Green et al., 2004; Ninomiya et al., 2004; Ninomiya and Winklbauer, 2008). Thus, non-canonical Wnt-signaling modulates both the formation and movement of F-actin contractions within the cortex of mesoderm cells.

Our description of punctuated actin contractions and observations of both F-actin morphology and changes in the dynamics following inhibition of actin polymerization or myosin II contractility suggest a complex model for punctuated contractions. In the first few seconds of a contraction, we observed F-actin moving towards the future center of the contraction, suggesting that myosin light chain activity is modulated within a small region of the sparse F-actin cortex. However, this slight movement of F-actin towards the focus does not appear to be sufficient to account for the rapid increase in F-actin as the contraction reaches its peak. To account for this increase and the results of our FRAP experiments, we propose a rapid increase in both polymerization and depolymerization of F-actin. The net effect of this ‘churning’ is to increase the abundance of F-actin within a contraction, but it does not change its lifetime. As the contraction dissipates, the rates of depolymerization must offset those of polymerization. The previous observation that F-actin is nearly absent after myosin-II-knockdown (Skoglund et al., 2008) is surprising, but this might reflect feedback mechanisms that adjust mechanical resistance to match the available generation of force (Davidson et al., 2009). The principle role of non-canonical Wnt-signaling is to control the frequency of contractions; however, Xfz7 can also subtly alter the dynamics of single contractions. This

model suggests that myosin activation might regulate F-actin polymerization in a manner similar to that described during single-cell wounding (Benink and Bement, 2005).

How might punctuated actin contractions drive convergent extension?

We can draw parallels between the role of actomyosin in regulating motility in single cells and its role in convergent extension. Actomyosin dynamics play essential roles in cell spreading (Senju and Miyata, 2009), polarized cell migration (Yam et al., 2007) and the establishment and maintenance of adherens junctions (Liu et al., 2010; Smutny et al., 2010). The events of single episodes of punctuated F-actin contractions are shared among many different cell types in *Xenopus* embryos; however, the frequency, localization and movements are not. For instance, contractions switch from having a randomly oriented movement to having a mediolaterally aligned movement as mesodermal cells elongate parallel to the mediolateral axis. We suggest several possibilities for how altered patterns of F-actin contraction might change cell shapes. First, aligned contractions might serve to reinforce the movement of a cell in the direction of contraction; mediolateral aligned contractions might allow mesodermal cells to better resist externally applied forces that would elongate the cell. Excessive mediolateral cell elongation could reduce the efficient conversion of mediolateral cell intercalation into convergent extension. An alternative function for contractions might be to enhance the rate of intercalation. Cycles of contraction aligned to the mediolateral axis could operate in a ratchet-like fashion, with cycles of cell adhesion driving mediolateral cell intercalation. None of these mechanisms are mutually exclusive, and oriented F-actin contractions could have several mechanical functions.

The punctuated F-actin contractions observed during morphogenesis in mesenchymal cells share many features with actin dynamics during epithelial morphogenesis. Many aspects of punctuated F-actin contractions are shared between the fly and frog, including: (1) the developmental control of contractions and coincidence of contractions with programmed cell-shape changes, (2) the restriction of high-frequency contractions to morphogenetically active cells, and (3) the duration of single contractions. However, contractions in *Xenopus* cells occur within the basolateral cortex of more loosely organized mesenchymal cells. Thus, our study supports the view that regulated F-actin contractions are a universal molecular mechanism for controlling embryonic cell shape, guiding programs of morphogenesis in both epithelial and mesenchymal tissues.

How might punctuated contractions regulate mediolateral cell intercalation and drive convergent extension? Early kinematic analyses of cell rearrangement during convergent extension in shaved-explants by Shih and Keller (Shih and Keller, 1992a; Shih and Keller, 1992b) indicate that the timescale of cell intercalation is very slow, so that each cell rearranges with neighbors only three to four times over the 6-hour course of gastrulation and axis elongation. The duty cycles of both protrusive activity and punctuated contractions are much shorter – on the scale of minutes. Thus, it is formally possible that each neighbor change is the net result of hundreds of actin contractions and hundreds of protrusions. Future work will need to overcome the experimental challenges and carry out more detailed cell mechanical analyses in order to resolve the physical mechanical contribution of punctuated contractions to cell elongation, cell intercalation and the events of convergent extension.

Developmental programs must regulate complex dynamics of actomyosin and the structures they form

Amphibian gastrulation movements require integrating forces from a variety of cellular sources, including tissue separation, radial intercalation, mesendoderm migration, mediolateral cell intercalation and ventral thickening, with the changing material properties and architecture of the embryo. Each tissue movement or cell behavior might require specially organized cortical actomyosin in each cell. How gene regulatory networks and patterns of growth factors achieve this task is largely unknown. We have shown here that balanced levels of myosin II contractility and a contiguous F-actin network are needed to support punctuated F-actin contractions during convergent extension. A recent study, on the effects of knocking down myosin IIA and myosin IIB, has also demonstrated the need for balanced myosin activity during convergent extension (Skoglund et al., 2008). In that study, a reduction in the level of myosin II also appeared to destabilize the F-actin cortex. In our studies, we observed graded changes in punctuated F-actin contractions from low to high myosin activities and from low to high F-actin polymerization rates. Future studies will be needed to dissect both the molecular and mechanical nature of punctuated contractions and to determine how physical and chemical cues in the embryo organize contractions within individual cells.

Materials and Methods

Embryo culture and explant preparation

Embryos were obtained by standard methods (Kay and Peng, 1991) and cultured to the desired stage (Nieuwkoop and Faber, 1967). Fertilized embryos were cultured in 1/3× modified Barth solution (MBS) (Sive et al., 2000). Embryos were selected at early gastrula (stage 10) and transferred into Danilchik's For Amy (DFA) medium supplemented with antibiotic and antimycotic (Sigma). The vitelline membranes were manually removed with sharpened forceps, and 180° marginal zone explants were microsurgically excised using hair-tools (Green et al., 2004). Marginal zone explants were mounted in a custom imaging chamber, prepared in advance with a fibronectin-coated glass substrate. Staging of explants was carried out by comparison with co-cultured whole embryos; references to early-, mid-, and late-gastrula refer to stage 10, 11 and 12, respectively.

Preparation of live-cell imaging probes

Capped mRNA encoding the actin-binding domain of moesin (moe–GFP), the actin-binding domain of utrophin (utrophin–GFP) or a membrane-targeted GFP (gap43–GFP) were transcribed (Epicentre; Madison WI) from linearized plasmids pCS107 and pCS2+. mRNA was purified using G50 chromatography and resuspended in RNase-free water at 0.1 μg/μl. Between 0.5 and 2.0 ng of mRNA (per embryo) was injected at multiple sites in one- to four-cell stage embryos. Embryos expressing the mRNA were then selected using a fluorescence-equipped stereoscope. Expression of tagged proteins had no effect on embryonic development through the tadpole stages (data not shown).

Histology and live imaging

To visualize F-actin morphology in fixed intact whole embryos or throughout the thickness of explants, we used the protocol described previously (Tao et al., 2005). Briefly, embryos were devitellined and transferred into fixative (fresh 3.7% paraformaldehyde and 0.25% glutaraldehyde in PBS with 0.1% Triton X-100) for 1 hour; marginal zone explants were fixed for 10 minutes. The embryos or explants were washed in PBST (PBS with 0.1% Triton X-100) for 30 minutes and incubated with BODIPY-FL–phallacidin (25:10,000) in PBST for 3 hours. After incubation, samples were washed for 30 minutes in PBST, then the embryos were bisected and the samples dehydrated in 100% isopropanol. Samples were cleared with Murray's clear (2:1; benzyl benzoate to benzyl alcohol) (Kay and Peng, 1991) and mounted within custom chambers constructed from nylon washers (Small Parts, Miami Lakes, FL) glued onto 170-μm-thick glass coverslips with fingernail polish (Sally Hanson, 'Hard as Nails').

To visualize cell shapes or cytoskeletal dynamics in live cells, fluorescent-protein-expressing marginal zone explants were rinsed in fresh DFA, transferred into a custom acrylic chamber (Kim and Davidson, 2010), positioned and gently compressed under a coverslip fragment held in place with silicone grease (High Vacuum, Dow Chemical). To observe F-actin morphology and polymerization dynamics, time-lapse sequences of moe–GFP were collected using a confocal laser scanning microscope (SP5; Leica Microsystems) with a 63× oil immersion objective. Time-lapse sequences were assembled from single images collected at 10-second intervals.

The F-actin cortex is extremely thin and lies within 0.2 μm of the plasma membrane; even minimal drift can shift the cortex from the focal-plane.

Image and statistical analysis

In order to quantify the F-actin dynamics and minimize experimenter bias we wrote custom macros using image-processing software [ImageJ 1.43, author Wayne Rasband (Abramoff et al., 2004)]. Automated image analysis allows fine description of F-actin dynamics within the sparse pericellular cortex. As with the algorithms for analysis of F-actin in lamellipodia (Danuser and Waterman-Storer, 2006), our approach could detect small changes in actin dynamics, but was tailored to capture the unique structural features of cortical F-actin contractions. Briefly, a cell is segmented by small hexagonal units. The 'contractile' status of each hexagon was determined by the fluorescence intensity of the moe–GFP within each hexagon. To determine the duration and spatial extent of a contraction we linked contractile hexagons from one time-point to the next or to adjacent contractile hexagons in the same time-lapse frame. Groups of linked hexagons were categorized as a single F-actin contraction and tracked. The movement and the changing morphology of F-actin contractions were then measured using standard techniques.

Statistical analyses were performed with commercial software (SPSS statistics 17.0, SPSS, Chicago, IL). The correlation between two time-series of cell areas and moe–GFP intensities was tested by cross-correlation (Box and Jenkins, 1976); the Pearson correlation was used to test correlations between the immobile fraction and the cortical actin intensity (Blalock, 1972). ANOVA and Student's *t*-tests were used to assess statistical differences between different drug treatments (Sokal and Rohlf, 1994).

Fluorescent recovery after photobleaching

FRAP experiments were performed on a confocal laser scanning microscope (SP5; Leica Microsystems) with a 63× oil immersion objective with a 2× zoom. Photobleaching was performed on a 7-μm-by-7-μm region of cell cortex with the 488-nm argon laser operating at 100% laser power (pre- and post- bleaching images were collected with 20% laser power). Photobleaching was achieved using a confocal scanned pattern for ~5 seconds (10 iterations with 0.536 seconds per scan). Fluorescence recovery was monitored for 30 additional frames at the same frame rate. Fluorescent intensity profiles over time were normalized to pre-bleach levels for each cell and analyzed with commercial curve-fitting software (MATLAB R2009, The MathWorks, Natick, MA) to calculate the immobile fraction of fluorophores and their characteristic recovery time (Axelrod et al., 1976). Although the F-actin morphology and density was changing, these changes were slow with respect to the timecourse of FRAP. Pre-bleaching, bleaching and fluorescence recovery requires 20 seconds, which is much shorter than the 120-second timecourse of most F-actin contractions. The timecourse of the FRAP experiment and the selection of a large bleach zone let us interpret FRAP results as if the actin network were static.

We thank James Wang, Partha Roy, and Phil LeDuc for helpful discussions and acknowledge the support of members of our laboratory, including Mickey von Dassow, Sagar Joshi, Callie Johnson and Jian Zhou. We are especially grateful for the molecular biology assistance of Lin Zhang. This study was supported by grants from the National Institutes of Health (HD044750), the National Science Foundation (IOS-0845775) and an American Heart Association Beginning Grant-in-Aid to L.A.D. We also thank John Wallingford (xdd1 and moesin–GFP), William Bement (mRFP–utrophin), Herbert Steinbeisser (Xfz7) and James Bamburg (LimK^{CA}) for sharing plasmid constructs. Deposited in PMC for release after 12 months.

Note added in proof

A recent report from Rauzi et al. (Rauzi et al., 2010) describes a contractile actin cortex similar to those observed in our study in *Xenopus*, and implicates a role for these contractions in driving germ-band elongation in *Drosophila*.

Supplementary material available online at
http://jcs.biologists.org/cgi/content/full/124/4/635/DC1

References

Abramoff, M. D., Magelhaes, P. J. and Ram, S. J. (2004). Image processing with ImageJ. *Biophotonics International* **11**, 36-42.
Amato, P. A. and Taylor, D. L. (1986). Probing the mechanism of incorporation of fluorescently labeled actin into stress fibers. *J. Cell Biol.* **102**, 1074-1084.
Axelrod, D., Koppel, D. E., Schlessinger, J., Elson, E. and Webb, W. W. (1976). Mobility measurement by analysis of fluorescence photobleaching recovery kinetics. *Biophys. J.* **16**, 1055-1069.
Benink, H. A. and Bement, W. M. (2005). Concentric zones of active RhoA and Cdc42 around single cell wounds. *J. Cell Biol.* **168**, 429-439.
Blalock, H. M. (1972). *Social Statistics*. New York: McGraw-Hill.
Blanchard, G. B., Murugesu, S., Adams, R. J., Martinez-Arias, A. and Gorfinkiel, N. (2010). Cytoskeletal dynamics and supracellular organisation of cell shape fluctuations during dorsal closure. *Development* **137**, 2743-2752.
Box, G. E. P. and Jenkins, G. M. (1976). *Time Series Analysis: Forecasting and Control*. San Francisco: Holden-Day.
Burkel, B. M., von Dassow, G. and Bement, W. M. (2007). Versatile fluorescent probes for actin filaments based on the actin-binding domain of utrophin. *Cell Motil. Cytoskeleton* **64**, 822-832.
Capelluto, D. G., Kutateladze, T. G., Habas, R., Finkielstein, C. V., He, X. and Overduin, M. (2002). The DIX domain targets dishevelled to actin stress fibres and vesicular membranes. *Nature* **419**, 726-729.
Charras, G. T. (2008). A short history of blebbing. *J. Microsc.* **231**, 466-478.
Danuser, G. and Waterman-Storer, C. M. (2006). Quantitative fluorescent speckle microscopy of cytoskeleton dynamics. *Annu. Rev. Biophys. Biomol. Struct.* **35**, 361-387.
Davidson, L. A., Hoffstrom, B. G., Keller, R. and DeSimone, D. W. (2002). Mesendoderm extension and mantle closure in *Xenopus laevis* gastrulation: combined roles for integrin alpha5beta1, fibronectin, and tissue geometry. *Dev. Biol.* **242**, 109-129.
Davidson, L. A., Dzamba, B. D., Keller, R. and Desimone, D. W. (2008). Live imaging of cell protrusive activity, and extracellular matrix assembly and remodeling during morphogenesis in the frog, *Xenopus laevis*. *Dev. Dyn.* **237**, 2684-2692.
Davidson, L. A., Joshi, S. D., Kim, H. Y., von Dassow, M., Zhang, L. and Zhou, J. (2009). Emergent morphogenesis: elastic mechanics of a self-deforming tissue. *J. Biomech.* **43**, 63-70.
Djiane, A., Riou, J., Umbhauer, M., Boucaut, J. and Shi, D. (2000). Role of frizzled 7 in the regulation of convergent extension movements during gastrulation in Xenopus laevis. *Development* **127**, 3091-3100.
Dzamba, B. J., Jakab, K. R., Marsden, M., Schwartz, M. A. and DeSimone, D. W. (2009). Cadherin adhesion, tissue tension, and noncanonical Wnt signaling regulate fibronectin matrix organization. *Dev. Cell* **16**, 421-432.
Edwards, D. C. and Gill, G. N. (1999). Structural features of LIM kinase that control effects on the actin cytoskeleton. *J. Biol. Chem.* **274**, 11352-11361.
Effler, J. C., Iglesias, P. A. and Robinson, D. N. (2007). A mechanosensory system controls cell shape changes during mitosis. *Cell Cycle* **6**, 30-35.
Frydman, H. M. and Spradling, A. C. (2001). The receptor-like tyrosine phosphatase lar is required for epithelial planar polarity and for axis determination within drosophila ovarian follicles. *Development* **128**, 3209-3220.
Goto, T., Davidson, L., Asashima, M. and Keller, R. (2005). Planar cell polarity genes regulate polarized extracellular matrix deposition during frog gastrulation. *Curr. Biol.* **15**, 787-793.
Green, J. B., Dominguez, I. and Davidson, L. A. (2004). Self-organization of vertebrate mesoderm based on simple boundary conditions. *Dev. Dyn.* **231**, 576-581.
Hyodo-Miura, J., Yamamoto, T. S., Hyodo, A. C., Iemura, S., Kusakabe, M., Nishida, E., Natsume, T. and Ueno, N. (2006). XGAP, an ArfGAP, is required for polarized localization of PAR proteins and cell polarity in Xenopus gastrulation. *Dev. Cell* **11**, 69-79.
Kay, B. K. and Peng, H. B. (1991). *Xenopus laevis: Practical Uses in Cell and Molecular Biology*. New York: Academic Press.
Khadka, D. K., Liu, W. and Habas, R. (2009). Non-redundant roles for Profilin2 and Profilin1 during vertebrate gastrulation. *Dev. Biol.* **15**, 396-406.
Kim, H. Y. and Davidson, L. A. (2010). Methods to investigate molecular mechanisms and cellular mechanics responsible for morphogenesis in Xenopus laevis embryos. In *Imaging in Developmental Biology: A Laboratory Manual* (ed. J. Sharpe and R. Wong). NY: Cold Spring Harbor Laboratory Press.
Kwan, K. M. and Kirschner, M. W. (2005). A microtubule-binding Rho-GEF controls cell morphology during convergent extension of Xenopus laevis. *Development* **132**, 4599-4610.
Lanzetti, L. (2007). Actin in membrane trafficking. *Curr. Opin. Cell Biol.* **19**, 453-458.
Lauffenburger, D. A. and Horwitz, A. F. (1996). Cell migration: a physically integrated molecular process. *Cell* **84**, 359-369.
Litman, P., Amieva, M. R. and Furthmayr, H. (2000). Imaging of dynamic changes of the actin cytoskeleton in microextensions of live NIH3T3 cells with a GFP fusion of the F-actin binding domain of moesin. *BMC Cell Biol.* **1**, 1.
Liu, J., Kaksonen, M., Drubin, D. G. and Oster, G. (2006). Endocytic vesicle scission by lipid phase boundary forces. *Proc. Natl. Acad. Sci. USA* **103**, 10277-10282.
Liu, W., Sato, A., Khadka, D., Bharti, R., Diaz, H., Runnels, L. W. and Habas, R. (2008). Mechanism of activation of the Formin protein Daam1. *Proc. Natl. Acad. Sci. USA* **105**, 210-215.
Liu, Z., Tan, J. L., Cohen, D. M., Yang, M. T., Sniadecki, N. J., Ruiz, S. A., Nelson, C. M. and Chen, C. S. (2010). Mechanical tugging force regulates the size of cell-cell junctions. *Proc. Natl. Acad. Sci. USA* **107**, 9944-9949.
Martin, A. C., Kaschube, M. and Wieschaus, E. F. (2009). Pulsed contractions of an actin-myosin network drive apical constriction. *Nature* **457**, 495-499.
Mlodzik, M. (2006). A GAP in convergent extension scores PAR. *Dev. Cell* **11**, 2-4.
Mseka, T., Bamburg, J. R. and Cramer, L. P. (2007). ADF/cofilin family proteins control formation of oriented actin-filament bundles in the cell body to trigger fibroblast polarization. *J. Cell Sci.* **120**, 4332-4344.
Munro, E., Nance, J. and Priess, J. R. (2004). Cortical flows powered by asymmetrical contraction transport PAR proteins to establish and maintain anterior-posterior polarity in the early C. elegans embryo. *Dev. Cell* **7**, 413-424.
Nieuwkoop, P. D. and Faber, J. (1967). *Normal Tables of Xenopus laevis (Daudin)*. Amsterdam: Elsevier North-Holland Biomedical Press.
Ninomiya, H. and Winklbauer, R. (2008). Epithelial coating controls mesenchymal shape change through tissue-positioning effects and reduction of surface-minimizing tension. *Nat. Cell Biol.* **10**, 61-69.

Ninomiya, H., Elinson, R. P. and Winklbauer, R. (2004). Antero-posterior tissue polarity links mesoderm convergent extension to axial patterning. *Nature* **430**, 364-367.
Ramos, J. W. and DeSimone, D. W. (1996). *Xenopus* embryonic cell adhesion to fibronectin: position-specific activation of RGD / Synergy site-dependent migratory behavior at gastrulation. *J. Cell Biol.* **134**, 1-14.
Ramos, J. W., Whittaker, C. A. and DeSimone, D. W. (1996). Integrin-dependent adhesive activity is spatially controlled by inductive signals at gastrulation. *Development* **122**, 2873-2883.
Rauzi, M., Lenne, P. F. and Lecuit, T. (2010). Planar polarized actomyosin contractile flows control epithelial junction remodelling. *Nature* **468**, 1110-1114.
Reichl, E. M., Ren, Y., Morphew, M. K., Delannoy, M., Effler, J. C., Girard, K. D., Divi, S., Iglesias, P. A., Kuo, S. C. and Robinson, D. N. (2008). Interactions between myosin and actin crosslinkers control cytokinesis contractility dynamics and mechanics. *Curr. Biol.* **18**, 471-480.
Rosenblatt, J., Raff, M. C. and Cramer, L. P. (2001). An epithelial cell destined for apoptosis signals its neighbors to extrude it by an actin- and myosin-dependent mechanism. *Curr. Biol.* **11**, 1847-1857.
Sato, A., Khadka, D. K., Liu, W., Bharti, R., Runnels, L. W., Dawid, I. B. and Habas, R. (2006). Profilin is an effector for Daam1 in non-canonical Wnt signaling and is required for vertebrate gastrulation. *Development* **133**, 4219-4231.
Senju, Y. and Miyata, H. (2009). The role of actomyosin contractility in the formation and dynamics of actin bundles during fibroblast spreading. *J. Biochem.* **145**, 137-150.
Shih, J. and Keller, R. (1992a). Cell motility driving mediolateral intercalation in explants of *Xenopus laevis*. *Development* **116**, 901-914.
Shih, J. and Keller, R. (1992b). Patterns of cell motility in the organizer and dorsal mesoderm of *Xenopus laevis*. *Development* **116**, 915-930.
Sive, H. L., Grainger, R. M. and Harland, R. M. (2000). *Early Development of Xenopus laevis: A Laboratory Manual*. Cold Spring Harbor, NY: Cold Spring Harbor Laboratory Press.
Skoglund, P., Rolo, A., Chen, X., Gumbiner, B. M. and Keller, R. (2008). Convergence and extension at gastrulation require a myosin IIB-dependent cortical actin network. *Development* **135**, 2435-2444.
Slattum, G., McGee, K. M. and Rosenblatt, J. (2009). P115 RhoGEF and microtubules decide the direction apoptotic cells extrude from an epithelium. *J. Cell Biol.* **186**, 693-702.
Smutny, M., Cox, H. L., Leerberg, J. M., Kovacs, E. M., Conti, M. A., Ferguson, C., Hamilton, N. A., Parton, R. G., Adelstein, R. S. and Yap, A. S. (2010). Myosin II isoforms identify distinct functional modules that support integrity of the epithelial zonula adherens. *Nat. Cell Biol.* **12**, 696-702.
Sokal, R. R. and Rohlf, F. J. (1994). *Biometry*. New York: W. H. Freeman and Company.
Spector, I., Shochet, N. R., Blasberger, D. and Kashman, Y. (1989). Latrunculins-novel marine macrolides that disrupt microfilament organization and affect cell growth: I. Comparison with cytochalasin D. *Cell Motil. Cytoskeleton* **13**, 127-144.
Tanegashima, K., Zhao, H. and Dawid, I. B. (2008). WGEF activates Rho in the Wnt-PCP pathway and controls convergent extension in Xenopus gastrulation. *EMBO J.* **27**, 606-617.
Tao, Q., Lloyd, B., Lang, S., Houston, D., Zorn, A. and Wylie, C. (2005). A novel G protein-coupled receptor, related to GPR4, is required for assembly of the cortical actin skeleton in early Xenopus embryos. *Development* **132**, 2825-2836.
Tao, Y. S., Edwards, R. A., Tubb, B., Wang, S., Bryan, J. and McCrea, P. D. (1996). beta-Catenin associates with the actin-bundling protein fascin in a noncadherin complex. *J. Cell Biol.* **134**, 1271-1281.
Velarde, N., Gunsalus, K. C. and Piano, F. (2007). Diverse roles of actin in C. elegans early embryogenesis. *BMC Dev. Biol.* **7**, 142.
Viktorinova, I., Konig, T., Schlichting, K. and Dahmann, C. (2009). The cadherin Fat2 is required for planar cell polarity in the Drosophila ovary. *Development* **136**, 4123-4132.
Wallingford, J. B. and Harland, R. M. (2002). Neural tube closure requires Dishevelled-dependent convergent extension of the midline. *Development* **129**, 5815-5825.
Wallingford, J. B., Rowning, B. A., Vogeli, K. M., Rothbacher, U., Fraser, S. E. and Harland, R. M. (2000). Dishevelled controls cell polarity during Xenopus gastrulation. *Nature* **405**, 81-85.
Winklbauer, R., Nagel, M., Selchow, A. and Wacker, S. (1996). Mesoderm migration in the Xenopus gastrula. *Int. J. Dev. Biol.* **40**, 305-311.
Winklbauer, R., Medina, A., Swain, R. K. and Steinbeisser, H. (2001). Frizzled-7 signalling controls tissue separation during Xenopus gastrulation. *Nature* **413**, 856-860.
Wozniak, M. A. and Chen, C. S. (2009). Mechanotransduction in development: a growing role for contractility. *Nat. Rev. Mol. Cell Biol.* **10**, 34-43.
Yam, P. T., Wilson, C. A., Ji, L., Hebert, B., Barnhart, E. L., Dye, N. A., Wiseman, P. W., Danuser, G. and Theriot, J. A. (2007). Actin myosin network reorganization breaks symmetry at the cell rear to spontaneously initiate polarized cell motility. *J. Cell Biol.* **178**, 1207-1221.
Zallen, J. A. and Wieschaus, E. (2004). Patterned gene expression directs bipolar planar polarity in Drosophila. *Dev. Cell* **6**, 343-355.
Zar, J. H. (1998). *Biostatistical Analysis*. Upper Saddle River, NJ: Prentice-Hall.
Zhou, J., Kim, H. Y. and Davidson, L. A. (2009). Actomyosin stiffens the vertebrate embryo during critical stages of elongation and neural tube closure. *Development* **136**, 677-688.
Zhou, J., Kim, H. Y., Wang, J. H. C. and Davidson, L. A. (2010). Macroscopic stiffening of embryonic tissues via microtubules, Rho-GEF, and assembly of contractile bundles of actomyosin. *Development* **137**, 2785-2794.

Table S1. Quantified dynamics of punctuated F-actin contractions in early and late mesoderm and ectoderm cells (means±s.d)

	Ectoderm	Early mesoderm	Late mesoderm
# of explants	6	6	6
# of cells	17	17	14
Cell shape (LTW)	1.45±0.23	1.91±0.47	3.69±1.15
Contractile area (%)	20±13	45±9	35±11
Rate of contractions (#/hr)	15.90	45.94	46.71
Life span (min) per Contraction	3.24±2.48	3.11±2.57	2.42±1.98
Distance (μm) per Contraction	11.42±7.38	18.50±21.03	18.49±25.62

Table S2. Quantified dynamics of punctuated F-actin contractions in Xfz7-expressing cells (means±s.d.)

	Early mesoderm		Animal cap ectoderm	
	control	**Xfz7**	**control**	**Xfz7**
# of explants	4	4	3	3
# of cells	12	12	15	15
Cell shape (LTW)	2.11±0.84	1.51±0.22	1.35±0.25	1.77±0.45
Contractile area (%)	41±13	37±11	18±16	45±10
Rate of contractions (#/hr)	40.5	36.5	8.8	40.8
Life span (min) per Contraction	2.53±2.08	4.40±3.43	2.24±2.05	2.36±2.08
Distance (μm) per Contraction	12.88±12.79	20.78±18	9.56±7.33	12.24±11.46

Table S3. Quantified dynamics of punctuated F-actin contractions in Xdd1-expressing cells (means±s.d)

	Late mesoderm		Animal cap ectoderm	
	control	Xdd1	control	Xdd1
# of explants	7	5	3	6
# of cells	12	15	16	18
Cell shape (LTW)	4.13±1.72	1.44±0.24	1.31±0.24	1.44±0.31
Contractile area (%)	33±11	23±15	14±7	18±23
Rate of contractions (#/hr)	45.5	18.8	14.63	15
Life span (min) per Contraction	2.14±0.95	2±0.97	2.33±2.48	1.29±2.09
Distance (μm) per Contraction	10.51±4.4	8.77±4.45	0.5±0.25	0.35±0.44